Computational Materials Science 111 (2016) 131–136

Contents lists available at ScienceDirect

Computational Materials Science

journal homepage: www.elsevier.com/locate/commatsci

Comparison study of numerical methods for solving the Allen–Cahn equation

Darae Jeong [a], Seunggyu Lee [a], Dongsun Lee [b], Jaemin Shin [c], Junseok Kim [a,*]

[a] Department of Mathematics, Korea University, Seoul 136-713, Republic of Korea
[b] Department of Mathematical Sciences, Ulsan National Institute of Science and Technology, Ulsan 689-798, Republic of Korea
[c] Institute of Mathematical Sciences, Ewha W. University, Seoul 120-750, Republic of Korea

ARTICLE INFO

Article history:
Received 21 June 2015
Received in revised form 27 July 2015
Accepted 3 September 2015
Available online 26 September 2015

Keywords:
Allen–Cahn equation
Finite difference
Explicit
Implicit
Crank–Nicolson
Unconditionally gradient stable

ABSTRACT

The goal of this paper is to present a brief review and a critical comparison of the performance of several numerical schemes for solving the Allen–Cahn equation representing a model for antiphase domain coarsening in a binary mixture. Explicit, fully implicit, Crank–Nicolson, and unconditionally gradient stable schemes are considered. In this paper, we show the solvability conditions of the numerical schemes and the decreasing property of total energy using eigenvalues of the Hessian matrix of the energy functional. We also present the pointwise boundedness of the numerical solution for the Allen–Cahn equation. To compare the accuracy and numerical efficiency of these methods, numerical experiments such as traveling wave and motion by mean curvature are performed. Numerical results show that Crank–Nicolson and nonlinearly stabilized splitting schemes are almost close to the analytic solution. However, if a large time step is used in the numerical test, we have only two results with linearly and nonlinearly stabilized splitting schemes in spite of having large gaps between analytic solution and numerical results. The other numerical schemes except for linearly and nonlinearly stabilized splitting schemes have unstable results when large time step is used.

1. Introduction

In this paper, we shall present a brief review and a critical comparison of the performance of several numerical schemes for solving the Allen–Cahn (AC) equation [1]:

$$\frac{\partial \phi(\mathbf{x},t)}{\partial t} = -\frac{F'(\phi(\mathbf{x},t))}{\epsilon^2} + \Delta\phi(\mathbf{x},t), \quad \mathbf{x}\in\Omega,\ 0<t\leqslant T, \tag{1}$$

where $\Omega \subset \mathbb{R}^d$ $(d=1,2,3)$ is a domain. $\phi(\mathbf{x},t)$ is the difference between the concentrations of the two mixtures' components and $F(\phi) = 0.25(\phi^2-1)^2$. The parameter ϵ is the gradient energy coefficient related to the interfacial energy. The boundary condition is

$$\mathbf{n}\cdot\nabla\phi = 0 \text{ on } \partial\Omega, \tag{2}$$

where $\mathbf{n}$ denotes the normal vector on $\partial\Omega$. The AC equation is the L^2-gradient flow of the following total free energy functional:

$$\mathcal{E}(\phi) = \int_\Omega \left(\frac{F(\phi)}{\epsilon^2} + \frac{1}{2}|\nabla\phi|^2\right) d\mathbf{x}. \tag{3}$$

Differentiating the energy $\mathcal{E}(\phi)$ with respect to t gives

$$\begin{aligned}\frac{d}{dt}\mathcal{E}(\phi) &= \int_\Omega \left(\frac{F'(\phi)}{\epsilon^2}\phi_t + \nabla\phi\cdot\nabla\phi_t\right) d\mathbf{x} \\ &= \int_\Omega \left(\frac{F'(\phi)}{\epsilon^2} - \Delta\phi\right)\phi_t\, d\mathbf{x} = -\int_\Omega (\phi_t)^2\, d\mathbf{x} \leqslant 0,\end{aligned} \tag{4}$$

where the integration by parts and the boundary condition (2) are used. Therefore, the total energy is non-increasing in time. The AC Eq. (1) was originally introduced as a mathematical model for antiphase domain coarsening in a binary alloy [1]. The equilibrium configuration of the Ginzburg–Landau free energy functional has been applied to a wide range of problems such as phase transitions [2], coupled with the Navier–Stokes equation [3,4], energy minimizers [5], a gradient flow of a lower semicontinuous convex function [6], the motion by mean curvature flows [7], image analysis [8–12], crystal growth [13], anisotropic equations [14,15], vector-valued Allen–Cahn equation [12,16,17], precipitation and dissolution [18], pattern dynamics of reaction–diffusion equations [19,20], and degenerate diffusion [21]. Error estimates and stability were also studied in [22,23]. In addition, high accuracy solution for the AC equation is discussed in [24,25] and the conservative AC equation is also studied [26,27].

* Corresponding author. Tel.: +82 2 3290 3077; fax: +82 2 929 8562.
E-mail addresses: tinayoyo@korea.ac.kr (D. Jeong), 509sky@hanmail.net (S. Lee), esen@unist.ac.kr (D. Lee), zmshin@korea.ac.kr (J. Shin), cfdkim@korea.ac.kr (J. Kim).
URL: http://math.korea.ac.kr/~cfdkim (J. Kim).

http://dx.doi.org/10.1016/j.commatsci.2015.09.005
0927-0256/

This paper is organized as follows. In Section 2, we describe numerical analysis such as solvability, the total energy decrease, and the boundedness of the numerical solution. We present the numerical results in Section 3. In Section 4, we conclude.

2. Numerical analysis

We present various numerical schemes for the AC equation. For simplicity, we discretize the AC equation in one-dimensional space $\Omega = (a, b)$. Higher dimensional discretizations are similarly defined. Let N be a positive even integer, $h = (b-a)/N$ be the uniform mesh size, and $\Omega_h = \{x_i = (i-0.5)h, 1 \leqslant i \leqslant N\}$ be the set of cell-centers. Let ϕ_i^n be approximations of $\phi(x_i, n\Delta t)$, where $\Delta t = T/N_t$ is the time step, T is the final time, N_t is the total number of time steps, and $\boldsymbol{\phi}^n = (\phi_1^n, \phi_2^n, \ldots, \phi_N^n)$. Let a discrete differentiation operator be $\nabla_h \phi^n_{i+\frac{1}{2}} = (\phi^n_{i+1} - \phi^n_i)/h$, then the zero Neumann boundary condition (2) is defined as

$$\nabla_h \phi^n_{\frac{1}{2}} = \nabla_h \phi^n_{N+\frac{1}{2}} = 0. \tag{5}$$

We then define a discrete Laplacian by $\Delta_h \phi_i = \left(\nabla_h \phi_{i+\frac{1}{2}} - \nabla_h \phi_{i-\frac{1}{2}}\right)\big/ h$ and discrete l_2-inner products by

$$\langle \boldsymbol{\phi}, \boldsymbol{\psi} \rangle_h = h\sum_{i=1}^{N} \phi_i \psi_i \quad \text{and} \quad (\nabla_h \boldsymbol{\phi}, \nabla_h \boldsymbol{\psi})_h = h\sum_{i=0}^{N} \nabla_h \phi_{i+\frac{1}{2}} \nabla_h \psi_{i+\frac{1}{2}}.$$

Note that a discrete summation by parts holds with the boundary condition (5), i.e., $\langle \Delta_h \boldsymbol{\phi}, \boldsymbol{\psi} \rangle_h = \langle \boldsymbol{\phi}, \Delta_h \boldsymbol{\psi} \rangle_h = -(\nabla_h \boldsymbol{\phi}, \nabla_h \boldsymbol{\psi})_h$. We also define the discrete norms as $\|\boldsymbol{\phi}\|_h^2 = \langle \boldsymbol{\phi}, \boldsymbol{\phi} \rangle_h$ and $\|\boldsymbol{\phi}\|_\infty = \max_{1 \leqslant i \leqslant N} |\phi_i|$. We consider the following six numerical schemes for Eq. (1) and compare their accuracy and performance by using numerical experiments:

$$\text{Explicit} \quad \frac{\phi_i^{n+1} - \phi_i^n}{\Delta t} = \frac{\phi_i^n - (\phi_i^n)^3}{\epsilon^2} + \Delta_h \phi_i^n, \tag{6}$$

$$\text{Implicit} \quad \frac{\phi_i^{n+1} - \phi_i^n}{\Delta t} = \frac{\phi_i^{n+1} - (\phi_i^{n+1})^3}{\epsilon^2} + \Delta_h \phi_i^{n+1}, \tag{7}$$

$$\text{Crank–Nicolson} \quad \frac{\phi_i^{n+1} - \phi_i^n}{\Delta t} = \frac{\phi_i^{n+1} - (\phi_i^{n+1})^3}{2\epsilon^2} + \frac{1}{2}\Delta_h \phi_i^{n+1} + \frac{\phi_i^n - (\phi_i^n)^3}{2\epsilon^2} + \frac{1}{2}\Delta_h \phi_i^n, \tag{8}$$

$$\text{Nonlinear splitting} \quad \frac{\phi_i^{n+1} - \phi_i^n}{\Delta t} = \frac{\phi_i^n - (\phi_i^{n+1})^3}{\epsilon^2} + \Delta_h \phi_i^{n+1}, \tag{9}$$

$$\text{Linear splitting} \quad \frac{\phi_i^{n+1} - \phi_i^n}{\Delta t} = \frac{3\phi_i^n - 2\phi_i^{n+1} - (\phi_i^n)^3}{\epsilon^2} + \Delta_h \phi_i^{n+1}, \tag{10}$$

where $i = 1, \ldots, N$.

2.1. Solvability of the schemes

Let us consider the following discrete AC equation:

$$\frac{\phi_i^{n+1} - \phi_i^n}{\Delta t} = \frac{-\alpha(\phi_i^{n+1})^3 - (1-\alpha)(\phi_i^n)^3 + \beta\phi_i^{n+1} + (1-\beta)\phi_i^n}{\epsilon^2} + \Delta_h(\gamma\phi_i^{n+1} + (1-\gamma)\phi_i^n), \tag{11}$$

where α, β, and γ are real numbers. Note that

$$\text{Explicit} \quad \alpha = \beta = \gamma = 0, \tag{12}$$

$$\text{Implicit} \quad \alpha = \beta = \gamma = 1, \tag{13}$$

$$\text{Crank–Nicolson} \quad \alpha = \beta = \gamma = \frac{1}{2}, \tag{14}$$

$$\text{Nonlinear splitting} \quad \alpha = 1,\ \beta = 0,\ \gamma = 1, \tag{15}$$

$$\text{Linear splitting} \quad \alpha = 0,\ \beta = -2,\ \gamma = 1. \tag{16}$$

Here, the explicit scheme is uniquely solvable in Eq. (11). Therefore, we focus on the solvability of the other four schemes.

Bearing in mind that we want to have Eq. (11) as the Euler equation of a functional, we consider the following functional

$$\begin{aligned} G(\boldsymbol{\phi}) = {} & \frac{1}{2\Delta t}\|\boldsymbol{\phi} - \boldsymbol{\phi}^n\|_h^2 \\ & + \left\langle \frac{\alpha\boldsymbol{\phi}^3}{4\epsilon^2} + \frac{(1-\alpha)(\boldsymbol{\phi}^n)^3}{\epsilon^2} - \frac{\beta\boldsymbol{\phi}}{2\epsilon^2} - \frac{(1-\beta)\boldsymbol{\phi}^n}{\epsilon^2}, \boldsymbol{\phi} \right\rangle_h \\ & + \frac{\gamma}{2}\|\nabla_h \boldsymbol{\phi}\|_h^2 + (1-\gamma)(\nabla_h \boldsymbol{\phi}^n, \nabla_h \boldsymbol{\phi})_h. \end{aligned} \tag{17}$$

Here, we define the notation by $\boldsymbol{\phi}\boldsymbol{\psi} = (\phi_1\psi_1, \phi_2\psi_2, \ldots, \phi_N\psi_N)$. Let $\boldsymbol{\phi}^*$ and $\boldsymbol{\psi} \neq \mathbf{0}$ be fixed vectors and s be a real number variable. We consider a quartic polynomial H in s by

$$\begin{aligned} H(s) = {} & G(\boldsymbol{\phi}^* + s\boldsymbol{\psi}) \\ = {} & G(\boldsymbol{\phi}^*) + s\left\langle \frac{\boldsymbol{\phi}^* - \boldsymbol{\phi}^n}{\Delta t} + \frac{\alpha(\boldsymbol{\phi}^*)^3}{\epsilon^2} + \frac{(1-\alpha)(\boldsymbol{\phi}^n)^3}{\epsilon^2} \right. \\ & \left. - \frac{\beta\boldsymbol{\phi}^*}{\epsilon^2} - \frac{(1-\beta)\boldsymbol{\phi}^n}{\epsilon^2} - \Delta_h(\gamma\boldsymbol{\phi}^* + (1-\gamma)\boldsymbol{\phi}^n), \boldsymbol{\psi} \right\rangle_h \\ & + s^2\left\langle \frac{\boldsymbol{\psi}}{2\Delta t} + \frac{(3\alpha(\boldsymbol{\phi}^*)^2 - \beta)\boldsymbol{\psi}}{2\epsilon^2} - \frac{\gamma\Delta_h\boldsymbol{\psi}}{2}, \boldsymbol{\psi} \right\rangle_h + s^3\left\langle \frac{\alpha\boldsymbol{\phi}^*\boldsymbol{\psi}^2}{\epsilon^2}, \boldsymbol{\psi} \right\rangle_h \\ & + s^4\left\langle \frac{\alpha\boldsymbol{\psi}^3}{4\epsilon^2}, \boldsymbol{\psi} \right\rangle_h. \end{aligned} \tag{18}$$

And the second derivative is derived as

$$H''(s) = \left(\frac{1}{\Delta t} - \frac{\beta}{\epsilon^2}\right)\langle \boldsymbol{\psi}, \boldsymbol{\psi} \rangle_h + \frac{3\alpha}{\epsilon^2}\langle (\boldsymbol{\phi}^* + s\boldsymbol{\psi})^2, \boldsymbol{\psi}^2 \rangle_h + \gamma\|\nabla_h \boldsymbol{\psi}\|_h^2. \tag{19}$$

If the parameters satisfy $\alpha \geqslant 0$, $\beta < \epsilon^2/\Delta t$, and $\gamma \geqslant 0$, then $H''(s)$ has a strictly positive value. It means that the polynomial H is strictly convex and $G(\boldsymbol{\phi})$ is bounded below. Thus, there is the unique minimizer $\boldsymbol{\phi}^*$, i.e., $G(\boldsymbol{\phi}^*) \leqslant G(\boldsymbol{\phi})$ for all $\boldsymbol{\phi}$. Since $\boldsymbol{\phi}^*$ is the critical point, we have,

$$\begin{aligned} H'(0) = \Bigg\langle & \frac{\boldsymbol{\phi}^* - \boldsymbol{\phi}^n}{\Delta t} + \frac{\alpha(\boldsymbol{\phi}^*)^3}{\epsilon^2} + \frac{(1-\alpha)(\boldsymbol{\phi}^n)^3}{\epsilon^2} - \frac{\beta\boldsymbol{\phi}^*}{\epsilon^2} - \frac{(1-\beta)\boldsymbol{\phi}^n}{\epsilon^2} \\ & - \gamma\Delta_h\boldsymbol{\phi}^* - (1-\gamma)\Delta_h\boldsymbol{\phi}^n, \boldsymbol{\psi} \Bigg\rangle_h = 0. \end{aligned} \tag{20}$$

Since Eq. (19) holds regardless of $\boldsymbol{\psi}$, we have

$$\begin{aligned} \frac{\boldsymbol{\phi}^* - \boldsymbol{\phi}^n}{\Delta t} = {} & \frac{-\alpha(\boldsymbol{\phi}^*)^3 - (1-\alpha)(\boldsymbol{\phi}^n)^3 + \beta\boldsymbol{\phi}^* + (1-\beta)\boldsymbol{\phi}^n}{\epsilon^2} \\ & + \Delta_h(\gamma\boldsymbol{\phi}^* + (1-\gamma)\boldsymbol{\phi}^{\mathbf{n}}). \end{aligned} \tag{21}$$

Next, we want to show that the minimizer is unique. Let us assume $\hat{\boldsymbol{\phi}}$ is another minimizer, i.e., $G(\hat{\boldsymbol{\phi}}) = G(\boldsymbol{\phi}^*)$ and $\boldsymbol{\psi} = \hat{\boldsymbol{\phi}} - \boldsymbol{\phi}^* \neq \mathbf{0}$. By using the strict convexity of H, we have

$$G(\boldsymbol{\phi}^* + 0.5\boldsymbol{\psi}) = H(0.5) < \frac{H(0) + H(1)}{2} = \frac{G(\boldsymbol{\phi}^*) + G(\hat{\boldsymbol{\phi}})}{2} = G(\boldsymbol{\phi}^*),$$

which leads to a contradiction that $\boldsymbol{\phi}^*$ is the minimizer.

For linearly and nonlinearly stabilized splitting schemes, $H''(s) > 0$ is satisfied with any time step size. Crank–Nicolson and implicit schemes holds if $\Delta t < 2\epsilon^2$ and $\Delta t < \epsilon^2$, respectively. From now on, we define the unique minimizer as $\boldsymbol{\phi}^{n+1}$ and it satisfies Eq. (21).

2.2. Stability of the schemes

A numerical scheme is defined to be unconditionally gradient stable if the discrete total free energy is non-increasing for any size of a time step Δt. Eyre's theorem [28] shows that an unconditionally gradient stable algorithm results for the AC equation if we can split the free energy appropriately into contractive and expansive parts,

$$\mathcal{E}(\phi)=\int_a^b\left(\frac{F(\phi)}{\epsilon^2}+\frac{1}{2}\phi_x^2\right)dx=\mathcal{E}_c(\phi)-\mathcal{E}_e(\phi) \tag{22}$$

and then treat the contractive part $\mathcal{E}_c(\phi)$ implicitly and the expansive part $\mathcal{E}_e(\phi)$ explicitly. The main purpose of this section is to show that Eqs. (9) and (10) inherit characteristic property such as a decrease in the total energy. To show the decrease in the discrete total energy, first, we define a discrete Lyapunov functional,

$$\mathcal{E}^h(\boldsymbol{\phi}^n)=\frac{h}{4\epsilon^2}\sum_{i=1}^{N}\left((\phi_i^n)^2-1\right)^2+\frac{h}{2}\sum_{i=1}^{N-1}\left|\nabla_h\phi_{i+\frac{1}{2}}^n\right|^2 \tag{23}$$

for each n. It is convenient to decompose $\mathcal{E}^h(\boldsymbol{\phi}^n)$ into three parts:

$$\mathcal{E}^{(1)}(\boldsymbol{\phi}^n)=\frac{h}{2\epsilon^2}\sum_{i=1}^{N}(\phi_i^n)^2,\quad \mathcal{E}^{(2)}(\boldsymbol{\phi}^n)=\frac{h}{2}\sum_{i=1}^{N-1}\left|\nabla_h\phi_{i+\frac{1}{2}}^n\right|^2,$$
$$\mathcal{E}^{(3)}(\boldsymbol{\phi}^n)=\frac{h}{4\epsilon^2}\sum_{i=1}^{N}((\phi_i^n)^4+1).$$

We define a decomposition of $\mathcal{E}^h(\boldsymbol{\phi}^n)$ as $\mathcal{E}_c^h(\boldsymbol{\phi}^n)=-\beta\mathcal{E}^{(1)}(\boldsymbol{\phi}^n)+\gamma\mathcal{E}^{(2)}(\boldsymbol{\phi}^n)+\alpha\mathcal{E}^{(3)}(\boldsymbol{\phi}^n)$ and $\mathcal{E}_e^h(\boldsymbol{\phi}^n)=(1-\beta)\mathcal{E}^{(1)}(\boldsymbol{\phi}^n)-(1-\gamma)\mathcal{E}^{(2)}-(1-\alpha)\mathcal{E}^{(3)}$ where α, β, and γ are real numbers as in (12)–(16), i.e., $\mathcal{E}^h(\boldsymbol{\phi}^n)=\mathcal{E}_c^h(\boldsymbol{\phi}^n)-\mathcal{E}_e^h(\boldsymbol{\phi}^n)$. The numerical scheme in Eq. (9) can be regarded as the form of a gradient of the discrete total energy, i.e.,

$$\frac{\phi_i^{n+1}-\phi_i^n}{\Delta t}=-\frac{1}{h}\nabla\mathcal{E}_c^h(\boldsymbol{\phi}^{n+1})_i+\frac{1}{h}\nabla\mathcal{E}_e^h(\boldsymbol{\phi}^n)_i,\quad \text{for } i=1,\dots,N. \tag{24}$$

Given the discrete energy functional $\mathcal{E}^{(i)}(\boldsymbol{\phi})$, one defines the Hessian $\mathbf{H}^{(i)}$ to be the Jacobian of the $\nabla\mathcal{E}^{(i)}(\boldsymbol{\phi})$ and hence the Hessian for $i=1,2,3$ is represented by

$$\begin{aligned}&\left\{\mathbf{H}^{(1)},\mathbf{H}^{(2)},\mathbf{H}^{(3)}\right\}\\&=\left\{\nabla^2\mathcal{E}^{(1)}(\boldsymbol{\phi}),\nabla^2\mathcal{E}^{(2)}(\boldsymbol{\phi}),\nabla^2\mathcal{E}^{(3)}(\boldsymbol{\phi})\right\}\\&=\left\{\frac{h}{\epsilon^2}\begin{pmatrix}1&&&0\\&1&&\\&&\ddots&\\0&&&1\end{pmatrix},\ h\begin{pmatrix}1&-1&&&0\\-1&2&-1&&\\&\ddots&\ddots&\ddots&\\&&-1&2&-1\\0&&&-1&1\end{pmatrix},\right.\\&\left.\frac{3h}{\epsilon^2}\begin{pmatrix}\phi_1^2&&&&0\\&\phi_2^2&&&\\&&\ddots&&\\&&&\phi_{N-1}^2&\\0&&&&\phi_N^2\end{pmatrix}\right\},\end{aligned}$$

where we have used the boundary condition in Eq. (5). The eigenvalues of $\mathbf{H}^{(1)}$, $\mathbf{H}^{(2)}$, and $\mathbf{H}^{(3)}$ are

$$\lambda_k^{(1)}=\frac{h}{\epsilon^2},\quad \lambda_k^{(2)}=\frac{4}{h}\sin^2\frac{(k-1)\pi}{2N},\quad \lambda_k^{(3)}=\frac{3h}{\epsilon^2}\phi_k^2, \tag{25}$$

where $k=1,2,\dots,N$, respectively. Note that all eigenvalues in (25) are non-negative. Let $\mathbf{v}_k=\mathbf{w}_k/|\mathbf{w}_k|$ be the orthonormal eigenvector corresponding to the eigenvalues $\lambda_k^{(2)}$ where $\mathbf{w}_k=\left(\cos\frac{(k-1)\pi}{2N},\cos\frac{3(k-1)\pi}{2N},\dots,\cos\frac{(2N-1)(k-1)\pi}{2N}\right)$, then $\boldsymbol{\phi}^{n+1}-\boldsymbol{\phi}^n$ can be expressed in terms of $\mathbf{v}_k$ as

$$\boldsymbol{\phi}^{n+1}-\boldsymbol{\phi}^n=\sum_{k=1}^{N}\alpha_k\mathbf{v}_k. \tag{26}$$

The decrease of the discrete energy functional is established in the following theorem: If $\boldsymbol{\phi}^{n+1}$ is the solution of Eq. (9) with a given $\boldsymbol{\phi}^n$, then

$$\mathcal{E}^h(\boldsymbol{\phi}^{n+1})\leqslant\mathcal{E}^h(\boldsymbol{\phi}^n). \tag{27}$$

Next, we prove Eq. (27). This inequality has been shown for the nonlinear gradient stabilized scheme in [29] and here we consider all five finite difference schemes. Using an exact Taylor expansion of $\mathcal{E}^h(\boldsymbol{\phi}^n)$ about $\boldsymbol{\phi}^{n+1}$ up to the second order, we have

$$\begin{aligned}\mathcal{E}^h(\boldsymbol{\phi}^{n+1})-\mathcal{E}^h(\boldsymbol{\phi}^n)&=\left\langle\frac{1}{h}\nabla\mathcal{E}^h(\boldsymbol{\phi}^{n+1}),\boldsymbol{\phi}^{n+1}-\boldsymbol{\phi}^n\right\rangle_h\\&\quad-\left\langle\frac{1}{2h}\nabla^2\mathcal{E}^h(\boldsymbol{\xi})(\boldsymbol{\phi}^{n+1}-\boldsymbol{\phi}^n),\boldsymbol{\phi}^{n+1}-\boldsymbol{\phi}^n\right\rangle_h,\end{aligned} \tag{28}$$

where $\boldsymbol{\xi}=\theta\boldsymbol{\phi}^n+(1-\theta)\boldsymbol{\phi}^{n+1}$ and $0\leqslant\theta\leqslant1$. For the first term of the right-hand side of Eq. (28), using Eq. (24) and the mean value theorem, we have

$$\begin{aligned}\left\langle\frac{1}{h}\nabla\mathcal{E}^h(\boldsymbol{\phi}^{n+1}),\boldsymbol{\phi}^{n+1}-\boldsymbol{\phi}^n\right\rangle_h&=\left\langle\frac{1}{h}\nabla\mathcal{E}_c^h(\boldsymbol{\phi}^{n+1})-\frac{1}{h}\nabla\mathcal{E}_e^h(\boldsymbol{\phi}^{n+1}),\boldsymbol{\phi}^{n+1}-\boldsymbol{\phi}^n\right\rangle_h\\&\quad-\left\langle\frac{\boldsymbol{\phi}^{n+1}-\boldsymbol{\phi}^n}{\Delta t}+\frac{1}{h}\nabla\mathcal{E}_c^h(\boldsymbol{\phi}^{n+1})-\frac{1}{h}\nabla\mathcal{E}_e^h(\boldsymbol{\phi}^n),\boldsymbol{\phi}^{n+1}-\boldsymbol{\phi}^n\right\rangle_h\\&\leqslant-\frac{1}{h}\left\langle\nabla\mathcal{E}_e^h(\boldsymbol{\phi}^{n+1})-\nabla\mathcal{E}_e^h(\boldsymbol{\phi}^n),\boldsymbol{\phi}^{n+1}-\boldsymbol{\phi}^n\right\rangle_h\\&=-\frac{1}{h}\left\langle\nabla\mathcal{E}_e^h(\boldsymbol{\eta})(\boldsymbol{\phi}^{n+1}-\boldsymbol{\phi}^n),\boldsymbol{\phi}^{n+1}-\boldsymbol{\phi}^n\right\rangle_h\\&=-\frac{1}{h}\left\langle\left[(1-\beta)\mathbf{H}^{(1)}-(1-\gamma)\mathbf{H}^{(2)}-(1-\alpha)\mathbf{H}^{(3)}\right]\right.\\&\quad\left.(\boldsymbol{\phi}^{n+1}-\boldsymbol{\phi}^n),\boldsymbol{\phi}^{n+1}-\boldsymbol{\phi}^n\right\rangle_h,\end{aligned} \tag{29}$$

where $\boldsymbol{\eta}=\theta\boldsymbol{\phi}^n+(1-\theta)\boldsymbol{\phi}^{n+1}$ and $0\leqslant\theta\leqslant1$. Also, for the second term of the right-hand side of Eq. (28), using $\mathcal{E}^h=-\mathcal{E}^{(1)}+\mathcal{E}^{(2)}+\mathcal{E}^{(3)}$, we have

$$\begin{aligned}&-\left\langle\frac{1}{2h}\nabla^2\mathcal{E}^h(\boldsymbol{\xi})(\boldsymbol{\phi}^{n+1}-\boldsymbol{\phi}^n),\boldsymbol{\phi}^{n+1}-\boldsymbol{\phi}^n\right\rangle_h\\&=\frac{1}{2h}\left\langle\left(\mathbf{H}^{(1)}-\mathbf{H}^{(2)}-\mathbf{H}^{(3)}\right)(\boldsymbol{\phi}^{n+1}-\boldsymbol{\phi}^n),\boldsymbol{\phi}^{n+1}-\boldsymbol{\phi}^n\right\rangle_h\\&\leqslant\frac{1}{2h}\left\langle\left(\mathbf{H}^{(1)}-\mathbf{H}^{(2)}\right)(\boldsymbol{\phi}^{n+1}-\boldsymbol{\phi}^n),\boldsymbol{\phi}^{n+1}-\boldsymbol{\phi}^n\right\rangle_h.\end{aligned} \tag{30}$$

From the equality (26), and inequalities (29) and (30), we have

$$\begin{aligned}&\mathcal{E}^h(\boldsymbol{\phi}^{n+1})-\mathcal{E}^h(\boldsymbol{\phi})^n\\&\leqslant\left\langle\left[\frac{2\beta-1}{2h}\mathbf{H}^{(1)}+\frac{1-2\gamma}{2h}\mathbf{H}^{(2)}+\frac{1-\alpha}{h}\mathbf{H}^{(3)}\right](\boldsymbol{\phi}^{n+1}-\boldsymbol{\phi}^n),\boldsymbol{\phi}^{n+1}-\boldsymbol{\phi}^n\right\rangle_h\\&=\sum_{k,l=1}^{N}\left\langle\left[\frac{2\beta-1}{2h}\lambda_k^{(1)}+\frac{1-2\gamma}{2h}\lambda_k^{(2)}+\frac{1-\alpha}{h}\lambda_k^{(3)}\right]\alpha_k\mathbf{v}_k,\alpha_l\mathbf{v}_l\right\rangle_h\\&=\sum_{k,l=1}^{N}\left\langle\left[\frac{2\beta-1}{2\epsilon^2}+\frac{2-4\gamma}{h^2}\sin^2\frac{(k-1)\pi}{2N}+\frac{3-3\alpha}{\epsilon^2}\eta_k^2\right]\alpha_k\mathbf{v}_k,\alpha_l\mathbf{v}_l\right\rangle_h\\&=\sum_{k=1}^{N}\left[\frac{2\beta-1}{2\epsilon^2}+\frac{2-4\gamma}{h^2}\sin^2\frac{(k-1)\pi}{2N}+\frac{3-3\alpha}{\epsilon^2}\eta_k^2\right]\alpha_k^2.\end{aligned} \tag{31}$$

If the right hand side of Eq. (31) is negative, it is guaranteed that the energy functional is non-increasing. Therefore, the nonlinearly stabilized splitting scheme ($\alpha=1,\beta=0,\gamma=1$) inherits the energy

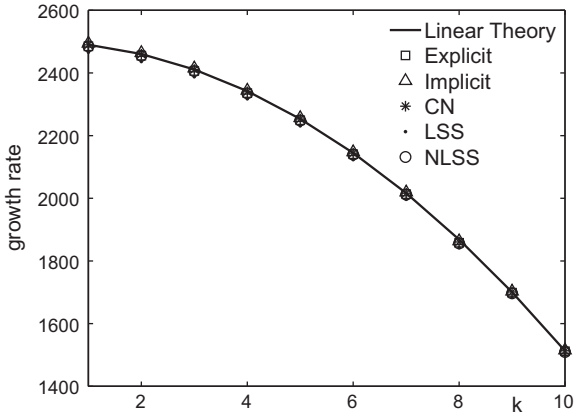

Fig. 1. Growth rate with different wave numbers.

non-increasing property. For the linearly stabilized splitting scheme $(\alpha = 0, \beta = -2, \gamma = 1)$, a sufficient condition for having negative value of Eq. (31) is $\eta_k \leqslant \sqrt{5/6}$.

2.3. Boundedness of the numerical solution

Next, we show that the decrease of the discrete total energy functional implies the pointwise boundedness of the numerical solution for the AC equation. If $\boldsymbol{\phi}^n$ is a numerical solution for the discrete AC equation and $\mathcal{E}^h(\boldsymbol{\phi}^n) \leqslant \mathcal{E}^h(\boldsymbol{\phi}^{n-1})$, then for any $1 \leqslant i \leqslant N$ we have

$$\frac{h}{4\epsilon^2}((\phi_i^n)^2 - 1)^2 \leqslant \mathcal{E}^h(\boldsymbol{\phi}^n) \leqslant \mathcal{E}^h(\boldsymbol{\phi}^0), \tag{32}$$

where we have used Eq. (23). Therefore, we have

$$||\boldsymbol{\phi}^n||_\infty \leqslant \sqrt{1 + 2\epsilon\sqrt{\mathcal{E}^h(\boldsymbol{\phi}^0)/h}}. \tag{33}$$

More details can be found in [29].

3. Numerical experiments

We define the width of the transition layer by using the ϵ value. From an equilibrium profile $\phi(x) = \tanh\left(x\Big/\left(\sqrt{2}\epsilon\right)\right)$, the concentration field ϕ varies from -0.9 to 0.9 over a distance of about $2\sqrt{2}\epsilon\tanh^{-1}(0.9)$. Therefore, if we want this value to be about mh [29], then we should take ϵ as

$$\epsilon_m = mh\Big/\left[2\sqrt{2}\tanh^{-1}(0.9)\right] \approx 0.24015mh. \tag{34}$$

3.1. Linear stability analysis

We perform a linear stability analysis [29,30]. Linearizing the AC Eq. (1) around $\phi \equiv 0$, then we have

$$\phi_t = \frac{\phi}{\epsilon^2} + \phi_{xx}. \tag{35}$$

If we assume $\phi(x,t) = \psi(t)\cos(k\pi x)$, where k is a wave number, then we get the following from Eq. (1)

$$\psi'(t)\cos(k\pi x) = -(k\pi)^2\psi(t)\cos(k\pi x) + \frac{\psi(t)\cos(k\pi x)}{\epsilon^2}.$$

Thus, $\psi(t) = \psi(0)e^{\lambda t}$, where $\lambda = 1/\epsilon^2 - (k\pi)^2$ is a growth rate. We also define the numerical growth rate by

$$\bar{\lambda} = \frac{1}{T}\log\left(\frac{\max_{1\leqslant i\leqslant N}|\phi_i^{N_t}|}{\psi(0)}\right).$$

The initial data is given by $\phi(x,0) = \psi(0)\cos(k\pi x)$ on the computational domain $\Omega = (0,1)$ with parameters $\epsilon = 0.02$, $N = 256$, $\psi(0) = 0.01$, $\Delta t = 0.1h^2$, and the final time $T = 100\Delta t$. Fig. 1 represents the linear stability tests of the five different schemes.

3.2. Decrease of the total energy

Next, we consider the evolution of the discrete total energy. The initial state is taken to be $\phi(x,0) = 0.1\text{rand}(x)$ on $\Omega = (0,1)$ with 64 grid points, rand(x) is a random number between -1 and 1. We use the simulation parameters ϵ_4 and $\Delta t = 0.2h^2$. In Fig. 2(a), the temporal evolution of the non-dimensional discrete total energy $\mathcal{E}^h(\boldsymbol{\phi}^n)/\mathcal{E}^h(\boldsymbol{\phi}^0)$ is shown. The total discrete energy is non-increasing. Also, the inscribed small figures are the concentration fields at the indicated times. Fig. 2(b) is a snapshot of $\phi(x,t)$ at $t = 0.001$.

3.3. Traveling wave solutions

One of the exact solutions of the AC equation is the traveling wave solution: $\phi(x,t) = 0.5 - 0.5\tanh\left[(x-st)\Big/\left(2\sqrt{2}\epsilon_4\right)\right]$, where $s = 3\Big/\left(\sqrt{2}\epsilon_4\right)$ is the speed of the traveling wave [29,31]. Now, we investigate the performance of the various numerical schemes such as explicit, fully implicit, CN, NLSS, and LSS methods on the traveling wave problem. For the numerical tests, we use the spatial step size $h = 11/512$ on $\Omega = (-1,10)$. Fig. 3(a) and (b) show the numerical solutions with two different time step sizes $\Delta t = 0.1h^2$ and $10h^2$ at $T = 140h^2$, respectively. Here, the analytic traveling wave solution at $t = T$ is represented by the solid line. In Fig. 3 (a), we have all five computational results with $\Delta t = 0.1h^2$. The result with CN method is almost identical with the analytic

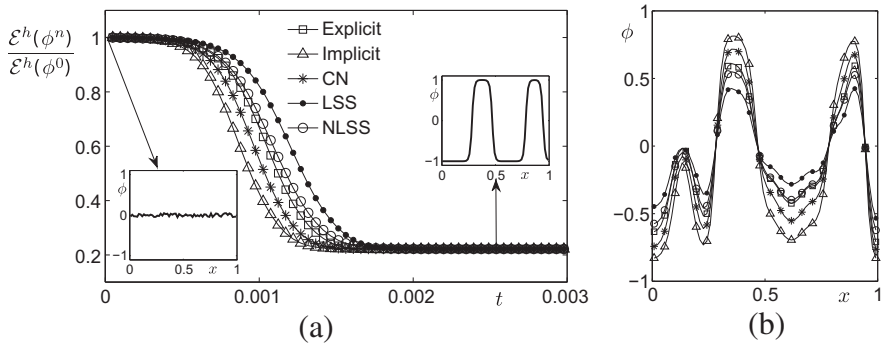

Fig. 2. (a) Temporal evolution of non-dimensional discrete total energy $\mathcal{E}^h(\boldsymbol{\phi}^n)/\mathcal{E}^h(\boldsymbol{\phi}^0)$ with an initial data, $\phi(x,0) = 0.1\text{rand}(x)$. (b) Snapshot of $\phi(x,t)$ at $t = 0.001$.

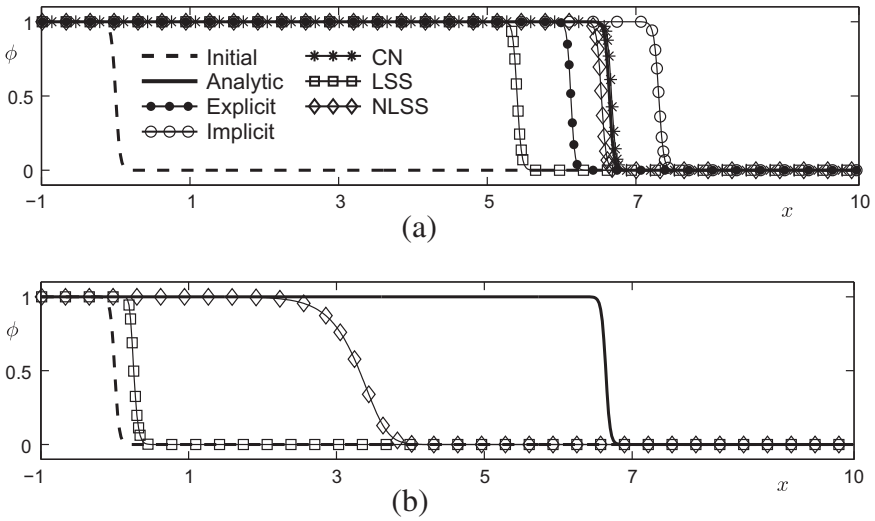

Fig. 3. Numerical traveling wave solutions with an initial profile $\phi(x,0) = \left(1 - \tanh\frac{x}{2\sqrt{2}\epsilon_4}\right)/2$ and two different time step sizes at final time $T = 140h^2$. (a) and (b) are results with $\Delta t = 0.1h^2$ and $10h^2$, respectively.

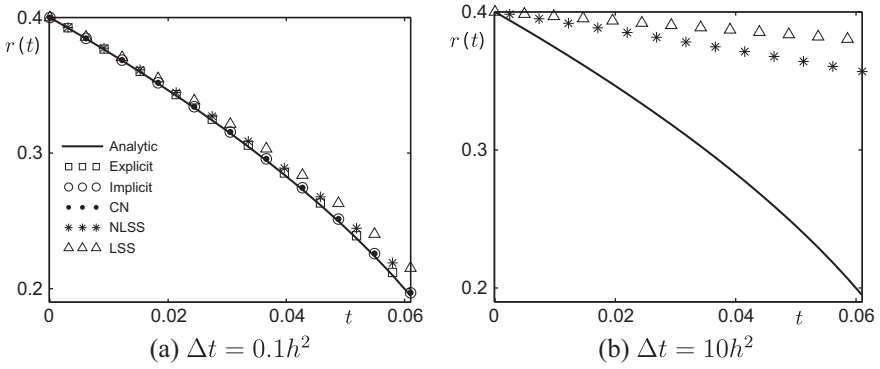

Fig. 4. Comparison of temporal evolutions of the radius with (a) $\Delta t = 0.1h^2$ and (b) $\Delta t = 10h^2$ from $t = 0$ to $t = 250h^2$ in two-dimensional space.

solution. NLSS is the third best among all. However, if we use a large time step $\Delta t = 10h^2$, then we have only NLSS and LSS results as shown in Fig. 3(b). However, there are large discrepancy between the analytic solution and numerical results with the large time step size. For NLSS case, interface transition profile is relaxed a lot. For LSS case, the actual evolution is small.

3.4. Motion by mean curvature

It was formally proved that, as $\epsilon \to 0$, the zero level set of ϕ evolves according to the geometric law

$$V = -\kappa = -\left(\frac{1}{R_1} + \frac{1}{R_2}\right), \tag{36}$$

where V is the normal velocity of the surface at each point, κ is its mean curvature, and R_1, R_2 are the principal radii of curvatures at the point of the surface [1]. In two-dimensional space, Eq. (36) becomes $V = -1/R$.

An initial condition is given as a circle with center $(0.5, 0.5)$ and radius $R_0 = 0.4$ on the computational domain $\Omega = (0,1) \times (0,1)$:

$$\phi(x,y,0) = \tanh\frac{R_0 - \sqrt{(x-0.5)^2 + (y-0.5)^2}}{\sqrt{2}\epsilon_8}. \tag{37}$$

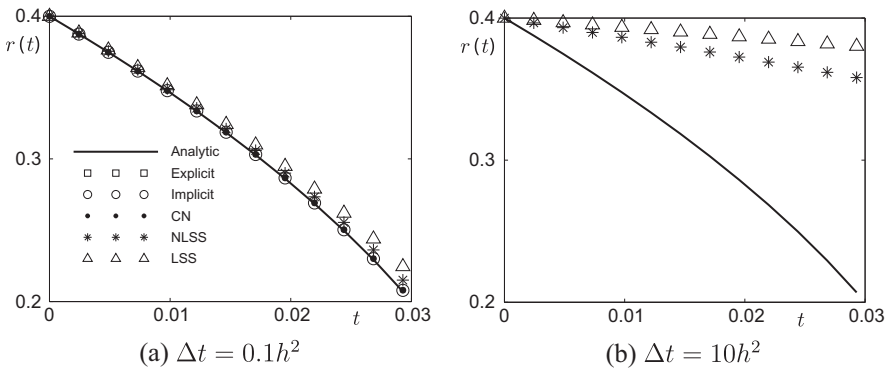

Fig. 5. Comparison of temporal evolutions of the radius with (a) $\Delta t = 0.1h^2$ and (b) $\Delta t = 10h^2$ up to $T = 120h^2$ in three-dimensional space.

Let R_0 and $R(t)$ be the initial radius and the radius at time t of the circle, respectively. Then Eq. (36) becomes $dR(t)/dt = -1/R(t)$. Therefore, analytic solution is given as $R(t) = \sqrt{R_0^2 - 2t}$. In order to compare the motion by curvature flow with several numerical schemes, we implement numerical simulations with ϵ_8, $h = 1/64$, and $T = 250h^2$. Fig. 4(a) and (b) show two results with $\Delta t = 0.1h^2$ and $\Delta t = 10h^2$, respectively.

When $\Delta t = 0.1h^2$, the numerical results with various schemes are close to analytic solution. With a large time step $\Delta t = 10h^2$, we have only two results with LSS and NLSS as shown in Fig. 4 (b) and we can see that the gaps between analytic and numerical results are large. The other schemes have unstable results with large time step size. Similarly, the radius of an sphere in three-dimensional space evolves with $R(t) = \sqrt{R_0^2 - 4t}$. The numerical results comparing with analytic solution are shown in Fig. 5. The behavior of numerical solutions is similar to results in the previous two-dimensional test. We used all same parameter values as the two-dimensional case except $T = 120h^2$.

4. Conclusions

In this paper, we reviewed and compared the performance of several numerical schemes for solving the Allen–Cahn equation representing a model for antiphase domain coarsening in a binary mixture. The numerical schemes we considered were explicit, fully implicit, Crank–Nicolson, and unconditionally gradient stable schemes. We showed the solvability and stability conditions of the numerical schemes. The continuous problem has a decreasing total energy and we showed the same property for the corresponding discrete problem by using eigenvalues of the Hessian matrix of the energy functional. We also showed the pointwise boundedness of the numerical solution for the Allen–Cahn equation. Numerical experiments such as traveling wave and motion by mean curvature were performed. The numerical results suggest that NLSS is best among the schemes in terms of stability and accuracy.

Acknowledgments

The first author (D. Jeong) was supported by Basic Science Research Program through the National Research Foundation of Korea (NRF) funded by the Ministry of Education, Science and Technology (2014R1A6A3A01009812). The third author (D. Lee) was supported by NRF (National Research Foundation of Korea) Grant funded by the Korean Government (NRF-2014-Fostering Core Leaders of the Future Basic Science Program). The corresponding author (J.S. Kim) was supported by the National Research Foundation of Korea (NRF) Grant funded by the Korea Government (MSIP) (NRF-2014R1A2A2A01003683).

References

[1] S.M. Allen, J.W. Cahn, Acta Metall. 27 (6) (1979) 1085–1095.
[2] M. Gokieli, L. Marcinkowski, Nonlinear Anal.-Theor. 63 (5) (2005) e1143–e1153.
[3] Y. Shi, X.P. Wang, Jpn. J. Ind. Appl. Math. 31 (3) (2014) 611–631.
[4] Q. Yang, B.Q. Li, J. Shao, Y. Ding, Int. J. Heat Mass Transfer 78 (2014) 820–829.
[5] T. Teramoto, Y. Nishiura, Jpn. J. Ind. Appl. Math. 27 (2) (2010) 175–190.
[6] M.H. GiGa, Y. GiGa, Jpn. J. Ind. Appl. Math. 27 (3) (2010) 323–345.
[7] X. Feng, A. Prohl, Numer. Math. 94 (1) (2003) 33–65.
[8] M. Beneš, V. Chalupecký, K. Mikula, Appl. Numer. Math. 51 (2) (2004) 187–205.
[9] J.A. Dobrosotskaya, A.L. Bertozzi, IEEE Trans. Image Process. 17 (5) (2008) 657–663.
[10] D.A. Kay, A. Tomasi, IEEE Trans. Image Process. 18 (10) (2009) 2330–2339.
[11] M. Rochery, I. Jermyn, J. Zerubia, in: ICCV 2005, Tenth IEEE International Conference on Computer Vision, 2005, vol. 2, IEEE, 2005, pp. 970–976.
[12] D. Kay, A. Tomasi, IEEE Trans. Image Process. 18 (10) (2009) 2330–2339.
[13] A.A. Wheeler, W.J. Boettinger, G.B. McFadden, Phys. Rev. A 45 (10) (1992) 7424–7439.
[14] C. Graäser, R. Kornhuber, U. Sack, IMA J. Numer. Anal. 33 (4) (2013) 1226–1244.
[15] B. Li, J. Lowengrub, A. Rätz, A. Voigt, Commun. Comput. Phys. 6 (3) (2009) 433–482.
[16] H.G. Lee, J. Kim, Comput. Phys. Commun. 183 (10) (2012) 2107–2115.
[17] R. Kornhuber, R. Krause, Comput. Vis. Sci. 9 (2) (2006) 103–116.
[18] Z. Xu, H. Huang, X. Li, P. Meakin, Comput. Phys. Commun. 183 (1) (2012) 15–19.
[19] M. Nagayama, K. Ueda, M. Yadome, Jpn. J. Ind. Appl. Math. 27 (2) (2010) 295–322.
[20] S. Ei, T. Ishimoto, Jpn. J. Ind. Appl. Math. 30 (1) (2013) 69–90.
[21] H.D. Ceniceros, C.J. García-Cervera, J. Comput. Phys. 246 (2013) 1–10.
[22] S. Bartels, Numer. Math. 99 (4) (2005) 557–583.
[23] S. Bartels, R. Müller, C. Ortner, SIAM J. Numer. Anal. 49 (1) (2011) 110–134.
[24] A. Christlieb, J. Jones, K. Promislow, B. Wetton, M. Willoughby, J. Comput. Phys. 257 (2014) 193–215.
[25] S. Zhai, X. Feng, Y. He, Comput. Phys. Commun. 185 (10) (2014) 2449–2455.
[26] J. Kim, S. Lee, Y. Choi, Int. J. Eng. Sci. 84 (2014) 11–17.
[27] S. Zhai, Z. Weng, X. Feng, Int. J. Heat Mass Transfer 87 (2015) 111–118.
[28] D.J. Eyre, An unconditionally stable one-step scheme for gradient systems. Unpublished article (1998). <http://www.math.utah.edu/~eyre/research/methods/stable.ps>.
[29] J.W. Choi, H.G. Lee, D. Jeong, J. Kim, Physica A 388 (9) (2009) 1791–1803.
[30] S. Gadkari, R. Thaokar, Int. J. Eng. Sci. 62 (2013) 9–21.
[31] A.M. Wazwaz, Appl. Math. Comput. 188 (2) (2007) 1467–1475.